International Journal of Nanomedicine

Dovepress
open access to scientific and medical research

Open Access Full Text Article

ORIGINAL RESEARCH

^{99m}Tc-radiolabeled composites enabling in vivo imaging of arterial dispersal and retention of microspheres in the vascular network of rabbit lungs, liver, and liver tumors

This article was published in the following Dove Medical Press journal:
International Journal of Nanomedicine

Ross W Stephens[1]
Gregory D Tredwell[1]
Karen J Knox[1]
Lee A Philip[1]
David W King[1]
Kelly M Debono[2]
Jessica L Bell[1]
Tim J Senden[1]
Marcel R Tanudji[3]
Jillean G Winter[3]
Stephanie A Bickley[3]
Michael J Tapner[3]
Stephen K Jones[3]

[1]The Biomedical Radiochemistry Laboratory, Department of Applied Mathematics, Research School of Physics and Engineering, Australian National University, Canberra, ACT, Australia; [2]Animal Services Division, Research School of Biology, Australian National University, Canberra, ACT, Australia; [3]Research and Development, Sirtex Medical Limited, Sydney, NSW, Australia

Correspondence: Gregory D Tredwell
Department of Applied Mathematics, Research School of Physics and Engineering, Australian National University, 60 Mills Road, Canberra, ACT 2600, Australia
Email greg.tredwell@anu.edu.au

Purpose: Selective internal radiation therapy (SIRT) is an effective treatment option for liver tumors, using Y-90-loaded polymer microspheres that are delivered via catheterization of the hepatic artery. Since Y-90 is a beta emitter and not conveniently imaged by standard clinical instrumentation, dosimetry is currently evaluated in each patient using a surrogate particle, ^{99m}Technetium-labeled macroaggregated albumin (^{99m}Tc-MAA). We report a new composite consisting of ^{99m}Tc-labeled nanoparticles attached to the same polymer microspheres as used for SIRT, which can be imaged with standard SPECT.

Methods: Carbon nanoparticles with an encapsulated core of ^{99m}Tc were coated with the polycation protamine sulfate to provide electrostatic attachment to anionic polystyrene sulfonate microspheres of different sizes (30, 12, and 8 μm). The in vivo stability of these composites was determined via intravenous injection and entrapment in the capillary network of normal rabbit lungs for up to 3 hours. Furthermore, we evaluated their biodistribution in normal rabbit livers, and livers implanted with VX2 tumors, following intrahepatic artery instillation.

Results: We report distribution tests for three different sizes of radiolabeled microspheres and compare the results with those obtained using ^{99m}Tc-MAA. Lung retention of the radiolabeled microspheres ranged from 72.8% to 92.9%, with the smaller diameter microspheres showing the lowest retention. Liver retention of the microspheres was higher, with retention in normal livers ranging from 99.2% to 99.8%, and in livers with VX2 tumors from 98.2% to 99.2%. The radiolabeled microspheres clearly demonstrated preferential uptake at tumor sites due to the increased arterial perfusion produced by angiogenesis.

Conclusion: We describe a novel use of radiolabeled carbon nanoparticles to generate an imageable microsphere that is stable in vivo under the shear stress conditions of arterial networks. Following intra-arterial instillation in the normal rabbit liver, they distribute in a distinct segmented pattern, with the smaller microspheres extending throughout the organ in finer detail, while still being well retained within the liver. Furthermore, in livers hosting an implanted VX2 tumor, they reveal the increased arterial perfusion of tumor tissue resulting from angiogenesis. These novel composites may have potential as a more representative mimic of the vascular distribution of therapeutic microspheres in patients undergoing SIRT.

Keywords: liver cancer, SIRT, radiolabeled microspheres, medical imaging

Introduction

Metastatic carcinoma commonly occurs in the liver from primary carcinomas of eg, the colonic mucosa.[1] The hepatic lesions are often multifocal and may occur on a

submit your manuscript | www.dovepress.com
Dovepress
http://dx.doi.org/10.2147/IJN.S187153

background of hepatitis or liver cirrhosis. Single tumors may be resected with the expectation of achieving prolonged survival, but multifocal or diffuse metastases are generally not operable, so that only 10%–15% of patients are eligible for surgery.[2] Further, of those patients who do undergo partial hepatectomy, a large proportion will develop recurrent tumors that are no longer resectable. The use of microspheres to deliver selective internal radiation therapy (SIRT) that produces measurable tumor regression[3] has therefore been a significant advancement in the treatment of liver cancer and has opened the possibility of prolonged survival.[4] SIR-Spheres® (SIR-Spheres is a registered trademark of Sirtex Medical Limited) ^{90}Y resin microspheres have a median diameter of 32.5 μm and lodge at limiting diameters in the arterial vessels supplying a tumor, where their loading of Yttrium-90 radioisotope delivers cytotoxic beta radiation.[5] Experimental studies have shown that the increased density of the angiogenic network at the periphery of metastatic tumors growing in the liver can result in a significantly higher dose delivery to the tumor tissue compared with the normal liver parenchyma.[6] Other microspheres that are used clinically are TheraSphere® (TheraSphere is a registered trademark of Theragenics Corporation), which is an insoluble glass microsphere containing Yttrium-90, and a recent product QuiremSpheres® (QuiremSpheres is a registered trademark of Quirem Medical BV), which consists of a poly-L-lactic acid microsphere and uses Holmium-166.

However, at least two factors can influence distribution of the microspheres in SIRT: firstly, the normal vessel divisions from the descending aorta to those ultimately supplying the liver have variations arising during embryological development;[7] secondly, the growth of a tumor in the liver and its associated angiogenesis can produce changes in the arterial network of the liver, sometimes resulting in a significant hepatopulmonary or hepatogastric shunting.[8] Administration of Y-90 microspheres into the liver's arterial network in liver cancer patients can thus present challenges in dosimetry, since while Yttrium-90 bremsstrahlung may correspond to the active tumor area, it does not give comparable resolution to SPECT with gamma emitting isotopes such as ^{99m}Tc.[9] Positron emission tomography–computed tomography imaging of ^{90}Y microspheres is rapidly evolving and proving to be a superior imaging modality over ^{90}Y Bremsstrahlung SPECT/CT. However, it is not yet widely employed due to varying success regarding quantitative accuracy, and the images that are produced are often inherently noisy due to the extremely small positron emission branching fraction of ^{90}Y.[10]

To predict organ distribution of SIR-Spheres microspheres prior to SIRT, it is a common practice to employ a surrogate radiolabeled particle preparation in an effort to mimic the potential distribution of the SIR-Spheres microspheres. Technetium-labeled heat-aggregated albumin (^{99m}Tc-MAA) is established in SIRT clinics as a suitable mimic for this purpose. While it is a polydisperse population of different sized aggregates, it has a median particle size similar to SIR-Spheres microspheres and can be imaged by standard SPECT techniques. A study of several commercial macroaggregated albumin reagent kits measured mean particle sizes ranging from 17.9 to 33.5 μm.[11] However, it has been noted that the distribution of ^{99m}Tc-MAA may not always accord with hepatic angiography,[12] and being an unstable aggregate of denatured protein particles, it may be subject to disaggregation during dispersal by the considerable shear forces in arterial networks.[13,14]

We have previously described the synthesis of nanoparticles comprising a core of ^{99m}Tc encapsulated in graphitic carbon that can be readily coated with polycations.[15] These cationic coatings facilitate binding of the nanoparticles to heparan sulfate in the capillary glycocalyx of the lungs,[16] and a coating of calf thymus histones consistently improved tumor uptake of the nanoparticles in a rabbit VX2 liver tumor model when injected arterially via the hepatic artery.[17] In this report, we demonstrate the application of cationized carbon nanoparticles as a stable electrostatic radiolabel for larger microspheres using the same polymer microspheres as used for SIRT. We have tested the stability of these composite microspheres and their vascular distribution in rabbit lungs, liver, and a rabbit VX2 model of liver tumors. We have also tested three different sizes of microspheres and compared imaging of the resulting liver distribution with that obtained using ^{99m}Tc-MAA.

Materials and methods

Nanoparticle synthesis

Carbon-caged ^{99m}Tc (FibrinLite [FL]) was synthesized as described in detail in US patent 8,778,300.[18] The nanoparticle technology employed was based on Technegas™, a radioactive aerosol preparation developed for diagnostic ventilation imaging of the lungs.[19] Vapor-phase particle sizing using an electrostatic particle classifier (TSI Inc., Shoreview, MN, USA) showed the aerosol comprises log-normal distributed particles with the bell curve centered on 150–350 nm, and negligible particles $<$100 nm or $>$400 nm. Electron microscope characterization shows metallic platelets surrounded by multiple lamellae of carbon.[20] Using the patented FL

process, sodium ^{99m}Tc-pertechnetate solution was loaded into a graphite crucible and after removing sodium chloride by sublimation at 1,650°C, the radioisotope was plasma ablated at 2,750°C into an argon gas stream. Aerosol nanoparticles were collected into water (6.0 mL) from the gas stream using a Browitt sonicating precipitator,[21] thus producing a stable colloidal dispersion of FL. The radioactive FL colloid was filtered through a 450 nm hydrophilic membrane (mixed cellulose ester; Millipore) before use. A typical preparation of FL contained approximately 5 µg/mL of graphitic carbon with a specific activity of 20 MBq/µg. FL nanoparticles are highly stable, and integrity of the radioisotope encapsulation is preserved under standard autoclave conditions of 20 minutes at 120°C.

In vitro assays of FL binding to polystyrene microwells

We have previously shown using a membrane filtration model and microwell binding assays that polycations such as polylysine bind to the surface of FL with high affinity.[15] Binding of these polycations to FL is also stable under in vivo conditions, as shown by our previous imaging studies of polycation-coated FL in the capillary network of rabbit lungs.[15] We have proposed[16] that binding is mediated by multisite pi–cation interactions[22,23] between the positively charged amino groups of the amino acid side-chains and the pi-electrons of the planar carbon rings of the graphite surface. The protamine family of proteins is also polycationic due to a high content of arginine and lysine residues.[24] In the present study, the change in adhesion properties of FL after surface treatment with protamine sulfate (PS; Sigma-Aldrich, Sydney, Australia) was tested by microwell binding as follows: FL (5 MBq) was added to serial dilutions of PS (20 to 0 µg/mL) in a 0.5 mM Tris acetate buffer (pH 7.2) and allowed to stand for 1 hour at 20°C. Each treatment mixture was then added to triplicate polystyrene microwells (LockWell MaxiSorp, Nunc, Denmark), and the FL was allowed to bind to the plastic surface for 30 minutes at 37°C with shaking. After rinsing the microwells three times with water, the bound radioactivity was measured by gamma counting of the separated individual wells in a Capintec well counter (Ramsey, NJ, USA).

FL binding to polystyrene sulfonate microspheres

Polystyrene sulfonate microspheres (MS) of three different sizes were used in this study: 32.5 µm (MS30), 12.1±1.5 µm (MS12), and 8.3±1.1 µm (MS8) median diameter ±1 standard deviation (Sirtex Medical Limited, Sydney, NSW, Australia). The MS (40 mg) were washed three times with water (6 mL) by centrifugation (2,000 rpm for 2 minutes) and resuspension before radiolabeling. Freshly prepared FL (260 MBq in 6 mL) was first treated with PS (20 µg/mL) for 30 minutes before addition to the final centrifuged pellet of washed MS. The PS-treated FL was then allowed to bind to the MS with gentle mixing for 30 minutes at 20°C, during which the color of MS changed from pale yellow to dark gray and the supernatant cleared. After separation of the resulting FL-MS by centrifugation, it was washed three times with water (6 mL) by centrifugation and resuspension. At each step, the radioactivity was measured in the supernatant, and the radioactivity in the final washed FL-MS was expressed as a percentage of the original radioactivity applied. The radiolabeling method employed in this study is the subject of US patent 9,381,262 granted on July 5, 2016.

Scanning electron microscopy (SEM) of FL adherent on the surface of microspheres

FL-MS30 prepared by the above method was prepared for SEM using sputter coating with gold and imaged using a Jeol model JSM-840 SEM instrument at the Westmead Centre for Oral Health, Sydney. Unlabeled and labeled microspheres were scanned for direct comparison of their surface features.

In vivo stability tests of FL-MS and ^{99m}Tc-MAA after entrapment in normal rabbit lungs

All rabbit procedures adhered to the National Health and Medical Research Council's Australian code for the care and use of animals for scientific purposes (Australian Government, eighth edition, 2013), and the experimental protocols were approved by the Australian National University (ANU) Animal Ethics Committee. Rabbit imaging studies were carried out using intubation to deliver ventilation anesthesia with isoflurane, so that biodistribution of radiolabel in live animals could be followed for up to 3 hours. Imaging of the anesthetized rabbits and their excised organs after 3 hours was performed with a Hawkeye Infinia SPECT-CT camera (GE Healthcare). To test the stability of the radiolabeled MS, suspensions of FL-MS30, FL-MS12, and FL-MS8 (110–170 MBq on 15 mg MS in 5 mL 5% dextrose) were injected intravenously into an ear vein, so that the MS were mechanically arrested at limiting diameters in the arterial network of the lungs. Note that when FL is coated with PS, the coated nanoparticles are not retained in the lungs by binding to the heparan sulfate in the vascular glycocalyx.[16]

The lung retention obtained with the three sizes of MS was compared with lung retention of the clinical lung diagnostic agent, ^{99m}Tc-MAA (110–170 MBq on 2.5 mg in 5 mL 5% dextrose; DraxImage, Quebec, Canada). Static 5 minutes acquisitions were made on a 1,024×1,024 matrix, approx. 10 minutes after injection of the MS and again every hour up to 3 hours. A blood sample (5 mL) was taken before the rabbit was euthanized by a lethal injection while still under anesthesia. The lungs and liver were then excised after tying off blood vessels to prevent leakage of the radioisotope, and the excised organs and blood sample were imaged separately using a 5 minute acquisition on a 1,024×1,024 matrix and utilizing the camera's zoom function (lungs and blood sample 4×, livers 3×, whole body 1×). Counts registered in the acquisitions were corrected for the background activity of the corresponding field, and the corrected counts were used for calculation of the percentage activity remaining in the lungs compared to the liver, blood, and carcass. The total blood volume and radioactivity were calculated assuming 60 mL of blood per kg of rabbit body weight. To generate the lung figures, the lung dicom image files were read into MATLAB (MathWorks, Natick, MA, USA), and for each of the image, the individual pixel count was divided by the total image counts and then scaled by a constant factor.

Arterial distribution of FL-MS and labeling stability in rabbit livers

Intrahepatic artery instillations of FL-MS30, FL-MS12, FL-MS8 (40 mg each), and ^{99m}Tc-MAA (2.5 mg) were performed by catheterization of the cystic artery and using pulses of the particle suspension (total 5 mL 5% dextrose, 110–170 MBq) interspaced with normal hepatic artery blood flow, so as to disperse the radiolabeled material throughout the liver with close to normal arterial blood perfusion conditions.[25] The MS were kept suspended by gentle agitation during instillation. Static 5 minutes acquisitions were made on a 1,024×1,024 matrix, approx. 10 minutes after administration of the imaging agent and again after 1 hour. One hour was considered sufficient for the stability test to be relevant to the time between instillation of ^{99m}Tc-MAA and imaging of human patients in clinical SIRT procedures. A blood sample (5 mL) was taken before the rabbit was euthanized by lethal injection while still under anesthesia. The lungs and liver were excised after tying off blood vessels to prevent leakage of the radioisotope, and the excised organs were imaged separately using a 5 minutes acquisition on a 1,024×1,024 matrix and utilizing the zoom function (lungs and blood sample 4×, livers 3×, whole body 1×). Counts registered in the acquisitions were corrected for the background activity of the corresponding field, and the corrected counts were used for calculation of the percentage activity stably retained in the liver compared with the other organs. To generate the liver figures, the liver dicom image files were read into MATLAB (MathWorks), and for each of the image, the individual pixel count was divided by the total image counts and then scaled by a constant factor.

Rabbit VX2 liver tumor model

The transplantable rabbit VX2 tumor[26] was a kind gift from Dr J Geschwind (Johns Hopkins University, Baltimore, MD, USA) and was maintained as a serial transplant on the hind limbs of New Zealand White rabbits. Liver implants of tumor tissue were made at a single site in one lobe by keyhole surgery under ventilation anesthesia with isoflurane and allowed to grow for 18–21 days before use of the rabbit in imaging experiments. At this stage of growth, the tumor was an oblate ellipsoid of maximum diameter 2 cm, still contained within the liver lobe and not involving the body wall or other organs. Macroscopically, the tumor usually had a white necrotic center, surrounded by a prominently vascularized peripheral growth zone.

Results

FL binding to polystyrene microwells and microspheres

FL pretreated with low microgram concentrations of the polycation PS readily bound to polystyrene microwells as shown in Figure 1A. Increasing concentrations of PS produced more binding until excess PS competed with coated FL for binding to the plastic microwell surface, so that there was an optimal protamine concentration of ~5 μg/mL before binding of FL decreased. Similarly, the cationic-coated FL-PS nanoparticles bound strongly through an electrostatic interaction to the anionic polystyrene sulfonate microspheres (MS), changing their color from pale yellow to dark gray. The resulting radiolabeled FL-MS was stable to subsequent repetitive washing with centrifugation and resuspension (Figure 1B). Closely similar results were obtained for the binding of PS-treated FL to the different sizes of MS tested, ie, MS30, MS12, and MS8. SEM of FL-MS30 showed distributed islands of FL adherent on the surface of the MS (Figure 1C), compared with the smooth surface of untreated MS (Figure 1D).

In vivo stability tests of FL-MS following entrapment in the vascular network of normal rabbit lungs

Intravenous injection of rabbits with suspensions of FL-MS30, FL-MS12, and FL-MS8 resulted in retention of the majority of radiolabel in the lungs over at least 3 hours,

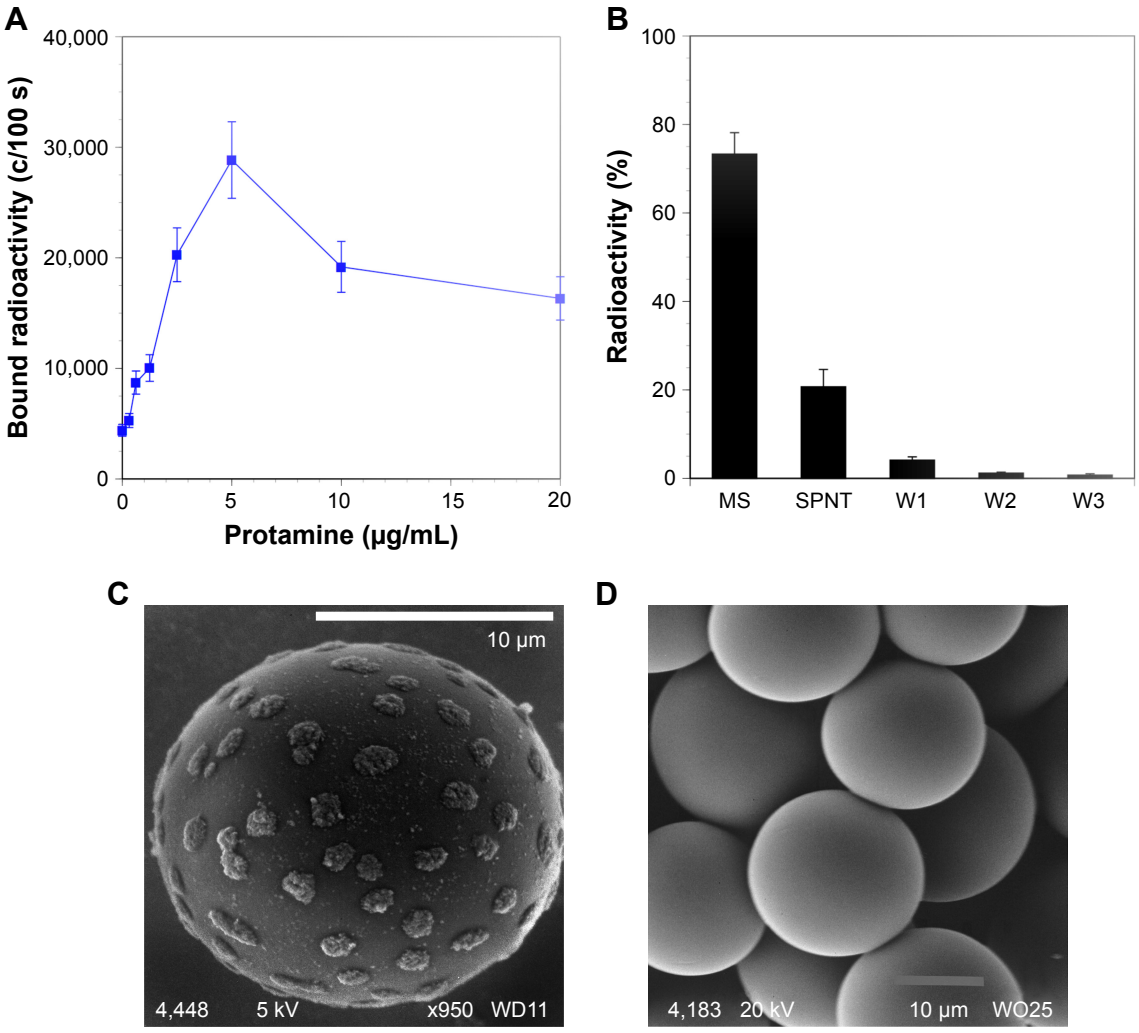

Figure 1 Binding of PS-treated FL to polystyrene MW and polystyrene sulfonate microspheres (MS).
Notes: Diluted FL (5 MBq; 1 mL) was treated for 1 hour with PS at the concentrations shown in **A**, before addition to triplicate MW. After binding for 30 minutes and rinsing three times with water, the MW were separated, and the bound radioactivity counted in each. In frame **B**, FL (400 MBq; 5 mL) was treated for 30 minutes with PS (5 µg/mL) before addition to prewashed MS of 30 µm diameter (40 mg). After binding for 30 minutes, the MS were rinsed three times and the bound radioactivity was measured and expressed as a percentage of the total applied. The mean values for six separate MS binding experiments are shown in **B**. Frame **C** is a scanning electron micrograph showing distributed islands of FL bound on the surface of an MS compared with plain MS in **D**.
Abbreviations: FL, FibrinLite; MS, polystyrene sulfonate microsphere; MW, microwells; PS, protamine sulfate; SPNT, supernatant; W1, wash 1 supernatant; W2, wash 2 supernatant; W3, wash 3 supernatant.

as shown by gamma camera imaging of the anesthetized animals (Figure 2A–C, respectively). FL-MS30 appeared to be more centralized in the lung images (Figure 2A), while the two smaller MS were widely dispersed in the lungs (Figure 2B and C). For comparison, rabbits were also injected intravenously with the clinical diagnostic agent used for imaging lung perfusion, ^{99m}Tc-MAA. As expected, this agent gave well-distributed imaging of the lungs (Figure 2D), but after 3 hours considerable label was apparent in the kidneys, presumably from free pertechnetate.[17]

More quantitative data for the stable retention of radiolabel in the lungs from each size of MS were obtained from imaging of a blood sample and the excised lungs, liver, and carcass after dissection of animals at 3 hours (Table 1). For FL-MS30, the mean lung proportion at dissection for three animals was 92.9%±1.5% of the total body activity and only 4.3% was in the excised liver and 0.84% in the total blood volume. After intravenous injection of three rabbits with FL-MS12, the mean lung proportion was 87.6%±2.5%, while 9.8% was in the liver and 0.66% in the total blood volume. The same test with FL-MS8 showed that 72.8%±1.9% of radioactivity had been retained in the lungs after 3 hours, while 23.1% had been taken up the liver, and 1.1% was in the total blood volume (Table 1). After injection of ^{99m}Tc-MAA and dissection at 3 hours, the lungs accounted for just 66.8%±5.7% of the total radioactivity from this agent, with 4.5% in the liver, and 29% in the carcass, which included the 8.2% present in the blood (Table 1). While escape of FL-MS8 from the lungs appeared to be in the form of particles captured by the reticuloendothelial system in the liver

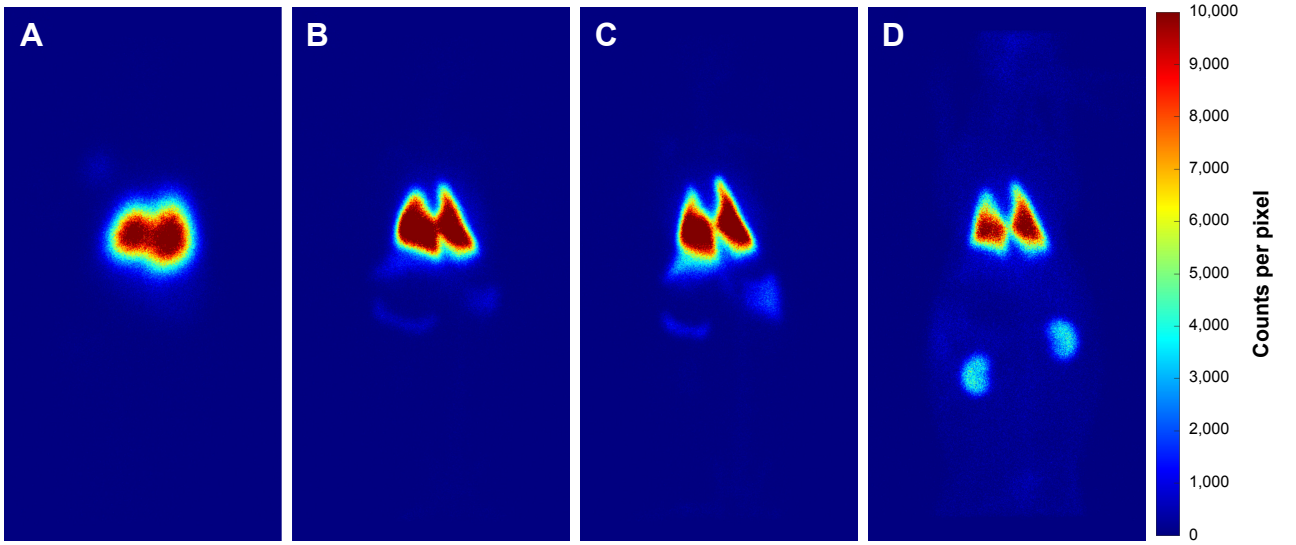

Figure 2 Lung stability tests of radiolabeled microspheres after intravenous injection in rabbits.
Notes: The frames **A**–**C** show gamma camera images of anesthetized normal rabbits taken 3 hours after intravenous injection of a 5% dextrose suspension (5 mL) containing 15 mg FL-MS30, FL-MS12, and FL-MS8 (130 MBq), respectively. Note the pronounced retention of the radiolabel in the lungs. For comparison, frame **D** shows a 3 hours post-injection image of a rabbit injected with the lung diagnostic agent ^{99m}Tc-MAA (2.5 mg, 130 MBq); note the activity in the lungs but also in the kidneys.
Abbreviations: ^{99m}Tc-MAA, ^{99m}Technetium-labeled macroaggregated albumin; FL, FibrinLite; MS, polystyrene sulfonate microspheres.

(Table 1), escape of ^{99m}Tc-MAA from the lungs produced visible labeling of the kidneys (Figure 2D) that was measured in the carcass (Table 1). This renal uptake was suggestive of soluble ^{99m}Tc-pertechnetate from the ^{99m}Tc-MAA preparation. By contrast, leaching of soluble radiolabel from FL-labeled MS appeared to be minimal.

Biodistribution and radiolabeling stability of FL-radiolabeled microspheres instilled intra-arterially in normal rabbit liver

Imaging of intact rabbits 1 hour after arterial instillation of FL-MS30 in the liver showed virtually complete retention of radiolabel in the organ. Imaging of three dissected animals showed a mean retention of 99.8% of the total radioactivity in the excised liver, while barely detectable levels in the excised lungs, and a blood sample verified that leaching of soluble radiolabel from MS and escape to other organs was negligible (Table 2). Imaging of the excised livers also revealed a pronounced, coarsely segmented distribution of the radiolabel within the organ (Figure 3A), which was markedly different from the previously reported uniform liver uptake of radiolabeled FL nanoparticles by the reticuloendothelial system[17] following intravenous or intra-arterial administration. Distribution of label did not extend throughout all areas of the organ and was highly variable between different livers. The appearance was of restricted distribution in which dispersal of FL-MS30 by the blood flow had been arrested at limiting diameters of the arterial network extending from the main feeder vessels, so that MS distribution was incomplete and clearly could not transit to the venous side.

Table 1 Stability test of radiolabeled MS and ^{99m}Tc-MAA in rabbit lungs following intravenous injection

MS/particle	Excised lungs (% total)	Excised liver (% total)	Carcass (% total)	Blood estimate (% total)
FL-MS30	92.9±1.5	4.3±0.5	2.8±1.1	0.84±0.1
FL-MS12	87.6±2.5	9.8±2.3	2.0±0.1	0.66±0.2
FL-MS8	72.8±1.9	23.1±1.6	2.9±0.4	1.1±0.03
^{99m}Tc-MAA	66.8±5.7	4.5±0.3	29±5.4	8.2±1.4

Notes: Biodistribution of radioactivity in rabbits 3 hours after intravenous (ear vein) injection of suspensions of FL-radiolabeled microspheres and the particulate imaging agent, ^{99m}Tc-MAA. The polymer microspheres (15 mg) had median diameters of 30 µm (FL-MS30), 12 µm (FL-MS12), and 8 µm (FL-MS8), and each 5 mL injection contained 130–170 MBq ^{99m}Tc. The clinical diagnostic imaging agent ^{99m}Tc-MAA (2.5 mg; 110–170 MBq) was also injected intravenously for comparison. The total radioactivity refers to the sum of lungs, liver, and carcass. A blood sample (5 mL) was taken prior to dissection for estimation of the radioactivity due to blood included in the carcass, assuming a blood volume of 60 mL per kg body weight. Images for measurement of radioactivity in the excised liver, lungs, blood sample, and carcass were acquired using a Hawkeye Infinia gamma camera (GE Healthcare). The results shown are the means and SEM of triplicate experiments for each type of MS/particle. All radioactivity measurements were corrected for background in the corresponding acquisition field. Note minimal leach of radiolabel from the MS into the blood compared with the leach from ^{99m}Tc-MAA.
Abbreviations: FL, FibrinLite; MS, polystyrene sulfonate microspheres; SEM, scanning electron microscopy; ^{99m}Tc, ^{99m}Technetium; ^{99m}Tc-MAA, ^{99m}Technetium-labeled macroaggregated albumin.

Table 2 Retention of radiolabeled MS and ^{99m}Tc-MAA in rabbit liver following intra-arterial instillation

Liver	MS/particle	N	Excised liver (% total)	Excised lungs (% total)	Carcass (% total)	Blood estimate (% total)	Tumor liver lobe (% liver)
Normal	FL-MS30	3	99.8±0.06	0.013±0.005	0.17±0.05	0.15±0.08	–
	FL-MS12	5	99.5±0.10	0.098±0.068	0.43±0.062	0.35±0.15	–
	FL-MS8	5	99.2±0.22	0.23±0.077	0.51±0.17	0.16±0.077	–
	^{99m}Tc-MAA	3	97.1±0.43	0.12±0.015	2.81±0.39	1.59±0.44	–
VX2	FL-MS30	2	99.2±0.05	0.037±0.002	0.81±0.04	0.31±0.07	32.0±2.2
	FL-MS12	3	98.8±0.47	0.11±0.046	1.08±0.53	0.25±0.10	32.9±7.4
	FL-MS8	4	98.2±0.36	1.39±0.38	0.44±0.13	0.16±0.09	31.3±5.1
	^{99m}Tc-MAA	2	98.1±0.30	0.10±0.008	1.77±0.28	1.01±0.06	33.0±8.0

Notes: Retention of radioactivity in normal rabbit livers and livers hosting VX2 tumor implants 1 hour after intra-arterial instillation of radiolabeled microspheres and ^{99m}Tc-MAA. N is the number of replicate experiments performed for each particle size. The polymer microspheres (40 mg) had median diameters of 30 μm (FL-MS30), 12 μm (FL-MS12), and 8 μm (FL-MS8), and each 5 mL instillation contained 130–170 MBq ^{99m}Tc. The clinical diagnostic imaging agent ^{99m}Tc-MAA (2.5 mg; 110–170 MBq) was also instilled intra-arterially for comparison. The total radioactivity refers to the sum of lungs, liver, and carcass. A blood sample (5 mL) was taken prior to dissection for estimation of the radioactivity due to blood included in the carcass, assuming a blood volume of 60 mL per kg body weight. Images for measurement of radioactivity in the excised liver, lungs, blood sample, and carcass were acquired using a Hawkeye Infinia gamma camera (GE Healthcare). The results shown are the means and SEM for each type of MS/particle. All radioactivity measurements were corrected for background in the corresponding acquisition field. Note high rates of retention in the liver 1 hour post instillation, for normal and tumor livers. '–' denotes not applicable.

Abbreviations: FL, FibrinLite; MS, polystyrene sulfonate microspheres; SEM, scanning electron microscopy; ^{99m}Tc-MAA, ^{99m}Technetium-labeled macroaggregated albumin.

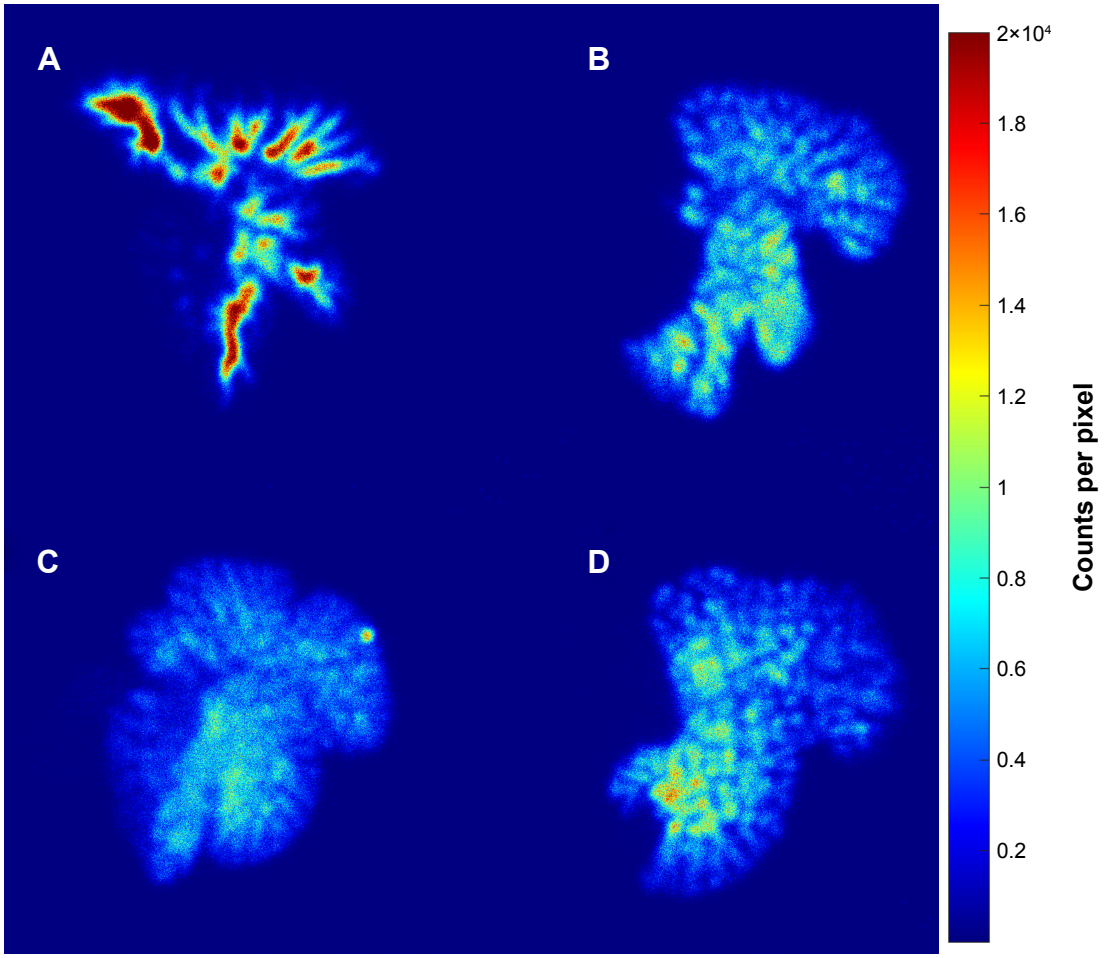

Figure 3 Distribution of radiolabeled microspheres and MAA in normal rabbit livers after intra-arterial instillation.

Notes: The frames **A–C** show gamma camera images of excised livers removed from normal rabbits 1 hour after intra-arterial instillation of a 5% dextrose suspension (5 mL) containing 40 mg FL-MS30, FL-MS12, and FL-MS8 (130 MBq), respectively. Note the increasing extent of dispersion of label in the organ with decreasing MS diameter. For comparison, frame **D** shows an excised liver removed from a rabbit 1 hour after intra-arterial instillation of ^{99m}Tc-MAA (2.5 mg, 130 MBq). Liver images were obtained using the camera's 3× zoom function.

Abbreviations: ^{99m}Tc-MAA, ^{99m}Technetium-labeled macroaggregated albumin; FL, FibrinLite; MS, polystyrene sulfonate microspheres.

Arterial instillation of FL-MS12 in the livers of five rabbits also showed strong retention of radiolabel after 1 hour; imaging of the excised livers gave a mean of 99.5% (Table 2). Distribution of radiolabel within the liver was noticeably different from FL-MS30, with more complete dispersal into the organ (Figure 3B). Interestingly, even the smallest MS, FL-MS8, was also well retained inside the liver for 1 hour (99.2%, Table 2), but the imaging of excised livers clearly showed a considerably more detailed and fine distribution of label extending throughout the organ, consistent with arrest of MS dispersal at a more distal limit of the liver's arterial network (Figure 3C). Escape of label to the lungs in these normal rabbits after 1 hour was <0.2% for all three sizes of MS, and leaching of soluble radiolabel to the blood was also very low (Table 2).

As expected from its mean diameter of 20–30 μm,[11] ^{99m}Tc-MAA was also well retained in the normal rabbit liver 1 hour after arterial instillation (97.1%; Table 2); however, imaging of the excised liver (Figure 3D) showed that the distribution of label was considerably more extensive and diffuse within the liver lobes than FL-MS30 (cf. Figure 3A), and more comparable with the finer structure revealed by FL-MS12 (cf. Figure 3C). The appearance of such an extensive distribution within the organ suggested that particles of this agent had reached finer vessels of the arterial network than by a particle diameter of 30 μm. While escape of label from ^{99m}Tc-MAA to the lungs after 1 hour remained very low at 0.12%, there was a noticeable activity in the blood (1.6%) that contributed to more than half of the carcass activity (2.8%; Table 2).

Biodistribution of FL-radiolabeled microspheres instilled intra-arterially in rabbit livers hosting an implant of VX2 tumor

The above tests with FL-MS30, FL-MS12, FL-MS8, and ^{99m}Tc-MAA were then repeated in rabbit livers hosting implants of the VX2 tumor, after 18–21 days of tumor growth. At the time of MS administration, tumors typically appeared as a single oblate ellipsoid of up to 2 cm diameter, thickening but still contained within the liver lobe and not involving the body wall or other organs. On sectioning, they usually had a white necrotic center, surrounded by a prominently vascularized peripheral zone. Hepatic artery instillation of FL-MS30 in two rabbits hosting such liver VX2 tumors resulted in 99.2% retention of radiolabel in the liver after 1 hour (Table 2); it was not noticeably less than the retention by a normal liver. Accordingly, leakage to the systemic circulation in these tumor rabbits was still very low, as shown in Table 2. The imaging of excised livers showed coarsely segmented features within the organ as in normal livers but the lobe hosting the tumor had accumulated noticeably more radiolabel than the rest of the liver (Figure 4A).

Arterial instillation of FL-MS12 also showed a strong retention of radiolabel in the tumor-bearing liver after 1 hour; imaging of the excised liver showed a mean of 98.8% of the total body activity (n=3; Table 2). As in normal livers, it was noticeable that dispersal of FL-MS12 label was more extensive in the organ than FL-MS30, reaching out to most of the lobes and occupying a larger proportion of the liver, but with a prominent accumulation of label at the tumor site (Figure 4B). Intra-arterial instillation of FL-MS8 into rabbit livers hosting VX2 tumors showed an even finer structure of the arterial network after 1 hour (Figure 4C) compared with Fl-MS30, and yet 98.2% of the total activity was still retained in the organ (n=4; Table 2). Accumulation of label at the tumor site featured prominently, and assumed the form of a bright, complete annulus at the angiogenic growth margin of the tumor, surrounding a lower intensity (necrotic) center (Figure 4C). Thus, a clearer definition of the tumor site in the whole animal (Figure 5) and its growth zone (Figure 4C) was considerably facilitated by the use of smaller MS, and without degradation of the liver retention.

Intra-arterial instillation of ^{99m}Tc-MAA into livers with tumors showed 98.1% retention of the total activity as in normal livers (n=2; Table 2) and accumulation of radioactivity at the tumor site (Figure 4D). While definition of the tumor growth zone was comparable with FL-MS12, it was not as clear as with FL-MS8.

Following the gamma camera imaging of rabbit livers containing the VX2 tumors, the host lobe was excised and imaged separately to determine if there was any preferential labeling of the tumors. With FL-MS30, the accumulation of label in the lobes hosting VX2 tumors represented an average 32.0% of the total liver uptake (Table 2). There was no difference in the accumulation of label in tumor lobes with FL-MS12 or FL-MS8, containing an average of 32.9% and 31.3% of the total liver uptake, respectively. Nor was there a difference with ^{99m}Tc-MAA where the average tumor lobe accumulation was 33.0%. The respective VX2 host lobes represented on average just 15.8% (range 11.9%–24.4%) of the liver weight. Thus, on a tissue weight basis, the tumor lobe received approximately double the radioactivity per gram of tissue compared with the rest of the liver.

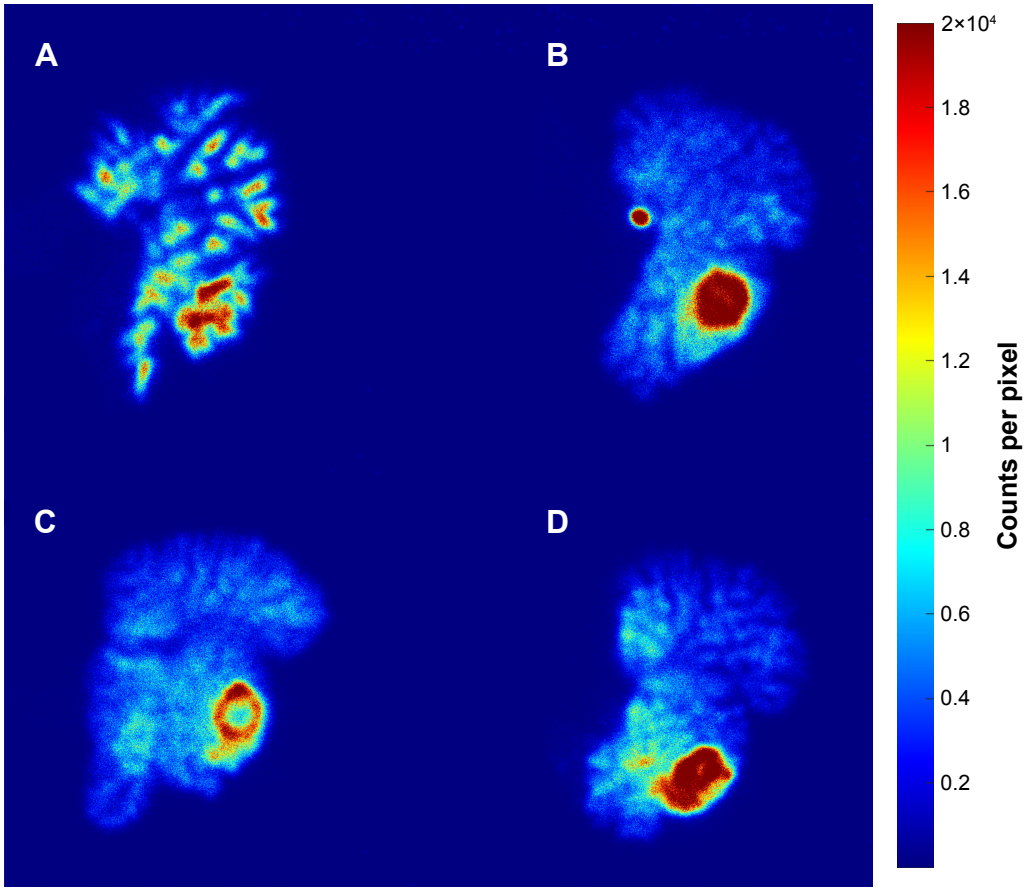

Figure 4 Distribution of radiolabeled microspheres and MAA in rabbit livers hosting a VX2 tumor implant.
Notes: The frames **A**–**C** show gamma camera images of excised livers with tumors removed from rabbits 1 hour after intra-arterial instillation of a 5% dextrose suspension (5 mL) containing 40 mg FL-MS30, FL-MS12, and FL-MS8 (130 MBq), respectively. Note the accumulation of label at the tumor site, with more pronounced definition of the angiogenesis zone by the smaller MS. For comparison, frame **D** shows an excised liver with tumor removed from a rabbit 1 hour after intra-arterial instillation of ^{99m}Tc-MAA (2.5 mg, 130 MBq). Liver images were obtained using the camera's 3× zoom function.
Abbreviations: ^{99m}Tc-MAA, ^{99m}Technetium-labeled macroaggregated albumin; FL, FibrinLite.

Discussion

Surface coating of FL with the polycation PS has previously been shown to produce a marked change in the adhesion properties of these nanoparticles, clearly evident in a membrane filtration model,[15] and this observation was exploited to bind FL through an electrostatic interaction to sulfonated polystyrene microspheres of the same type as used in SIRT. PS-coated FL bound avidly to the MS so that radiolabel was

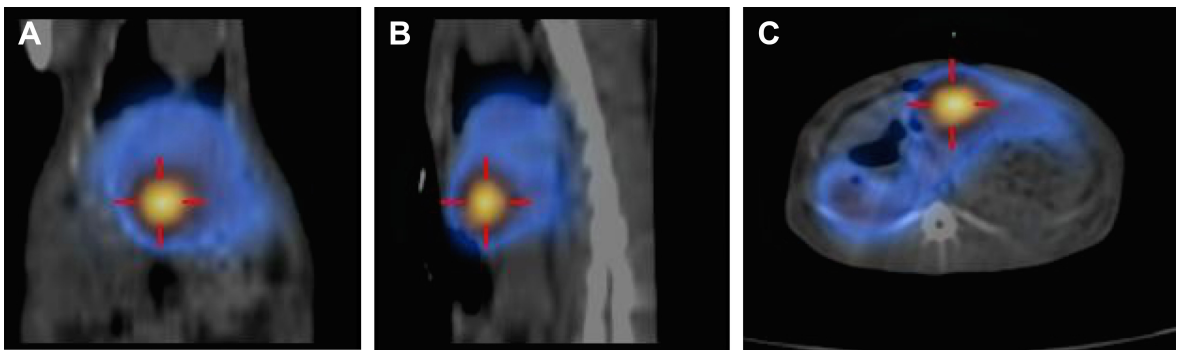

Figure 5 Liver VX2 tumor imaging in an intact rabbit with FL-MS8.
Note: The frames **A**–**C** show fused SPECT+ CT images for the coronal, sagittal and transaxial views respectively of an anesthetized rabbit with a liver implant of a VX2 tumor, 1 h after intra-arterial instillation of FL-MS8 (40 mg; 130 MBq). The accumulation of the radiolabelled microspheres at the tumor site (red cross) is clearly evident. The images are fused SPECT (color) + CT (gray scale) images. The whole body images were using the 1× zoom function.
Abbreviations: FL, FibrinLite; MS, polystyrene sulfonate microspheres.

well retained after successive washing steps, and this simple process provided specific activity levels of radioisotope that were more than sufficient to enable in vivo gamma camera imaging of three sizes of FL-MS after administration to anesthetized rabbits.

Leach tests of FL-MS30 lodged in the vascular network of rabbit lungs demonstrated that the radiolabel had excellent stability in vivo and persisted longer in the lungs than the lung diagnostic agent ^{99m}Tc-MAA. The ^{99m}Tc-MAA is known to be unstable in both lungs and the liver over time with a mean residence time in the lungs of 4 hours.[13,14] However, retention of nanoparticle radiolabel on the microspheres was virtually complete under these in vivo blood flow conditions so that very little radioactivity reached other organs over a 3 hours timecourse. The same tests with FL-MS12 and FL-MS8 showed that retention diminished somewhat with decreasing microsphere diameter, and slow loss of FL-MS8 from the lungs was observed, with significant label appearing in the liver after 3 hours. Nevertheless, lung retention of even FL-MS8 was appreciable, given that 10 μm is commonly accepted as being the lower limit of particle size required for retention in the lung capillary network.

Hepatic artery instillation of FL-MS30 into the rabbit liver showed very efficient retention of this preparation at limiting diameters of the liver arterial network, producing a coarse segmented distribution in imaging, consistent with the distributing arterioles within the organ. Arterial instillation of the smaller microspheres produced a noticeably different distribution of label, with finer features extending out to fill more of each liver lobe. The diameter of the microspheres was clearly an important property determining distribution in the arterial network of the organ. The larger microspheres reached a relatively proximal limiting diameter in the arterial supply, and as a consequence of this limited dispersal throughout the tissue, a higher radioactivity density was observed in the scaled images (Figure 3A). That is, the same radioactivity dose was contained within a smaller volume of tissue with FL-MS30 compared with the other microspheres. The smaller microspheres were carried further on to more distal limits, producing a finer featured distribution image with a lower radioactivity density. However, retention of even the smallest microspheres in the liver was surprisingly efficient; transit of radiolabel from the liver to other organs was very low and leaching of soluble radiolabel into blood was also very low. While it is difficult to extrapolate these results to humans as there may be differences in the size and length of human vs rabbit capillaries,[27] these are impressive results that demonstrate the stability of this radiolabeling method under in vivo conditions.

^{99m}Tc-MAA, while nominally of similar particle size to FL-MS30, and well retained in the liver after arterial instillation, nevertheless produced an image showing more extensive dispersal of label within the liver than that obtained with FL-MS30. This could suggest that the particle integrity of ^{99m}Tc-MAA was not maintained under arterial blood flow conditions in the liver and that it was disaggregated by shear forces to produce smaller particles.

When a VX2 tumor was present in the liver, instillation of all radiolabeled particles resulted in varying degrees of accumulation at the tumor site compared with the rest of the liver; the presence of a tumor effectively remodeled the arterial supply so as to favor tumor perfusion at the expense of arterial circulation to the rest of the liver. While there was no difference for tumor lobe accumulation between the different-sized microspheres, tumor definition on imaging, however, was most evident using FL-MS8. The tumor often featured as a remarkably intense annulus around the tumor set against a fine-featured background. This provided superior visual distinction of the active growth zone of the tumor compared with the coarse segmented pattern obtained with FL-MS30, and also compared with imaging with ^{99m}Tc-MAA.

In our series of rabbit liver tumor experiments, hepatopulmonary or hepatogastric shunting was not in evidence and retention of radiolabel within livers hosting a tumor was maintained at a very high level. Systemic release of radiolabel was not appreciably more than that seen in the case of normal livers, and even with the smallest diameter microspheres tested, the lungs had received only 1.4% of the radioactivity 1 hour after instillation of these microspheres in the tumor-bearing liver. This was comparable with systemic escape of radiolabel to the blood from ^{99m}Tc-MAA administered intra-arterially in normal and tumor-bearing livers.

Conclusion

Polymer microspheres of the type used for internal radiation therapy in liver cancer patients were conveniently radiolabeled at a specific activity suitable for imaging in vivo, using electrostatic attachment of protamine-coated nanoparticles comprising a carbon-encapsulated ^{99m}Tc core. This method of radiolabeling provided a stable composite in vivo under the shear stress conditions experienced in arterial networks of the lungs and liver in rabbit models. In the normal rabbit liver, arrest of radiolabeled microspheres at limiting diameters of arterial vessels showed increasing dispersal

and definition of network structure with decreasing size of the microspheres used. In livers hosting model tumors, the radiolabeled microspheres clearly demonstrated preferential uptake at tumor sites due to the increased arterial perfusion produced by angiogenesis. This result was most evident with microspheres of 8 μm diameter, which also provided clearest definition of the tumor growth zone while still being well retained within the liver. We did not find evidence of hepatopulmonary shunting from livers hosting model tumors.

Data sharing statement

The raw data required to reproduce these findings are available to download from Mendeley Data (doi: 10.17632/5hpzd4g524.1).

Acknowledgments

The ANU authors acknowledge the collaborative project support generously provided to ANU by Sirtex Medical Limited (Sydney), including donation of a GE Hawkeye Infinia SPECT/CT scanner and a Xeleris image processing system. We thank Mara Cvejic of the Westmead Centre for Oral Health, Sydney, for scanning electron microscopy of microsphere preparations. We also thank Gary Somerville of Cyclomedica Pty Ltd for assistance with Technegas™ equipment, and Dr Bill Burch, the inventor of Technegas, for helpful discussions. This work was funded through a collaborative research agreement with Sirtex Medical Limited, Sydney, Australia.

Disclosure

The radiolabeling method employed in this study is the subject of US patent 9,381,262, granted July 5, 2016. MRT, JGW, SAB, MJT, and SKJ are employed by Sirtex Medical Limited. The authors report no other conflicts of interest in this work.

References

1. van den Eynden GG, Majeed AW, Illemann M, et al. The multifaceted role of the microenvironment in liver metastasis: biology and clinical implications. *Cancer Res*. 2013;73(7):2031–2043.
2. Garrean S, Muhs A, Bui JT, et al. Complete eradication of hepatic metastasis from colorectal cancer by yttrium-90 SIRT. *World J Gastroenterol*. 2007;13(21):3016–3019.
3. Gray BN, Anderson JE, Burton MA, et al. Regression of liver metastases following treatment with yttrium-90 microspheres. *Aust N Z J Surg*. 1992;62(2):105–110.
4. Kucuk ON, Soydal C, Lacin S, Ozkan E, Bilgic S. Selective intraarterial radionuclide therapy with yttrium-90 (Y-90) microspheres for unresectable primary and metastatic liver tumors. *World J Surg Oncol*. 2011;9(1):86.
5. Burton MA, Gray BN, Klemp PF, Kelleher DK, Hardy N. Selective internal radiation therapy: distribution of radiation in the liver. *Eur J Cancer Clin Oncol*. 1989;25(10):1487–1491.
6. Campbell AM, Bailey IH, Burton MA. Tumour dosimetry in human liver following hepatic yttrium-90 microsphere therapy. *Phys Med Biol*. 2001;46(2):487–498.
7. Hiatt JR, Gabbay J, Busuttil RW. Surgical anatomy of the hepatic arteries in 1000 cases. *Ann Surg*. 1994;220(1):50–52.
8. Jiang M, Nowakowski FS, Wang J, et al. Characterization of extrahepatic distribution of Tc-99m macroaggregated albumin in hepatic perfusion imaging studies prior to yttrium-90 microsphere therapy. *Cancer Biother Radiopharm*. 2011;26(4):511–518.
9. Tehranipour N, Al-Nahhas A, Canelo R, et al. Concordant F-18 FDG PET and Y-90 bremsstrahlung scans depict selective delivery of Y-90-microspheres to liver tumors: confirmation with histopathology. *Clin Nucl Med*. 2007;32(5):371–374.
10. D'Arienzo M, Filippi L, Bagni O. Quantitative postradioembolization imaging using PET/CT. In: Pasciak AS, McKinney JM, Bradley YC, editors. *Handbook of Radioembolization*. Boca Raton, FL: Taylor & Francis Group; 2016:1–24.
11. Hung JC, Redfern MG, Mahoney DW, Thorson LM, Wiseman GA. Evaluation of macroaggregated albumin particle sizes for use in pulmonary shunt patient studies. *J Am Pharm Assoc*. 2000;40(1):46–51.
12. Kucuk ON, Soydal C, Araz M, Ozkan E, Aras G. Evaluation of the response to selective internal radiation therapy in patients with hepatocellular cancer according to pretreatment $^{(99m)}$Tc-MAA uptake. *Clin Nucl Med*. 2013;38(4):252–255.
13. Blau M, Wicks R, Thomas SR, Lathrop KA. Radiation absorbed dose from albumin microspheres labeled with technetium-99m. *J Nucl Med*. 1982;23(10):915–917.
14. Grosser OS, Ruf J, Kupitz D, et al. Pharmacokinetics of ^{99m}Tc-MAA- and ^{99m}Tc-HSA-microspheres used in preradioembolization dosimetry: influence on the liver-lung shunt. *J Nucl Med*. 2016;57(6):925–927.
15. Lobov SA, King DW, Knox KJ, Senden TJ, Stephens RW. Cationised radiolabelled nanoparticles for perfusion imaging of the lungs. *Biomaterials*. 2013;34(6):1732–1738.
16. Freeman CG, Parish CR, Knox KJ, et al. The accumulation of circulating histones on heparan sulphate in the capillary glycocalyx of the lungs. *Biomaterials*. 2013;34(22):5670–5676.
17. Stephens RW, Knox KJ, Philip LA, et al. The uptake of soluble and nanoparticulate imaging isotope in model liver tumours after intravenous and intra-arterial administration. *Biomaterials*. 2015;39:218–224.
18. Browitt RJ, Ba B, Burch WM, et al. Method of forming an injectable radioactive composition of a carbon encapsulated radioactive particulate. US Patent 8778300B2. 2014 July 15.
19. Browitt RJ, Burch WM, Senden TJ. Process for the production of a radioactive aerosol. US Patent 7722856B2. 2010 May 25.
20. Senden TJ, Moock KH, Gerald JF, et al. The physical and chemical nature of Technegas. *J Nucl Med*. 1997;38(8):1327–1333.
21. Browitt R, inventor; allrad No 19 Pty Ltd, assignee. United States patent US5792241A. 1994.
22. Ma JC, Dougherty DA. The cation–π interaction. *Chem Rev*. 1997;97(5):1303–1324.
23. Gallivan JP, Dougherty DA. Cation-pi interactions in structural biology. *Proc Natl Acad Sci U S A*. 1999;96(17):9459–9464.
24. Balhorn R. The protamine family of sperm nuclear proteins. *Genome Biol*. 2007;8(9):227.
25. Moroz P, Jones SK, Winter J, Gray BN. Targeting liver tumors with hyperthermia: ferromagnetic embolization in a rabbit liver tumor model. *J Surg Oncol*. 2001;78(1):22–29.
26. Lee KH, Liapi E, Buijs M, et al. Considerations for implantation site of VX2 carcinoma into rabbit liver. *J Vasc Interv Radiol*. 2009;20(1):113–117.
27. Doerschuk CM, Beyers N, Coxson HO, Wiggs B, Hogg JC. Comparison of neutrophil and capillary diameters and their relation to neutrophil sequestration in the lung. *J Appl Physiol*. 1993;74(6):3040–3045.